8-1-2008

Mapping and quantifying hyperpolarized 3He magnetic resonance imaging apparent diffusion coefficient gradients

Andrea Evans

David G McCormack

Giles Santyr

Grace Parraga

J Appl Physiol 105: 693–699, 2008.
First published June 5, 2008; doi:10.1152/japplphysiol.00178.2008.

Mapping and quantifying hyperpolarized ^{3}He magnetic resonance imaging apparent diffusion coefficient gradients

Andrea Evans,[1,2] David G. McCormack,[3,4] Giles Santyr,[1,2,5] and Grace Parraga[1,2,4,5]

[1]*Imaging Research Laboratories, Robarts Research Institute;* [2]*Department of Medical Biophysics,* [3]*Division of Respirology, Department of Medicine;* [4]*Lawson Health Research Institute; and* [5]*Department of Radiology and Nuclear Medicine University of Western Ontario, London, Canada*

Submitted 14 February 2008; accepted in final form 30 May 2008

Evans A, McCormack DG, Santyr G, Parraga G. Mapping and quantifying hyperpolarized ^{3}He magnetic resonance imaging apparent diffusion coefficient gradients. *J Appl Physiol* 105: 693–699, 2008. First published June 5, 2008; doi:10.1152/japplphysiol.00178.2008.—We measured hyperpolarized ^{3}He magnetic resonance imaging (MRI) apparent diffusion coefficients (ADC) and quantified ADC gradients in each three-by-three voxel region of interest (ROI). Such local ADC gradients can be represented in vector maps showing the magnitude ($|G_{3\times3}|$) and direction of ADC gradients, providing a qualitative visualization tool and quantitative measurement of airway and air space heterogeneity. Twenty-four subjects (15 male, mean age = 67 ± 7 yr) with global initiative for chronic obstructive lung disease (GOLD) stage II ($n = 9$, mean age 68 ± 6 yr), GOLD stage III chronic obstructive pulmonary disease (COPD; $n = 7$, mean age 67 ± 8 yr), and age-matched healthy volunteers ($n = 8$, mean age 67 ± 6 yr) were enrolled based on their age and spirometry results. Hyperpolarized ^{3}He MRI was performed on a whole body 3.0 Tesla system. Mean ^{3}He ADC and ADC standard deviation were calculated for the center coronal slice, and the mean magnitude and direction of the ADC gradient vectors were calculated for each three-by-three voxel matrix ($|G_{3\times3}|$). While the ^{3}He ADC standard deviation was not significantly different, mean $|G_{3\times3}|$ was significantly different between subjects with stage II (0.14 ± 0.03 cm/s) and stage III COPD (0.19 ± 0.03 cm/s; $P < 0.005$) and between healthy subjects (0.12 ± 0.03 cm/s) and those with stage II COPD ($P < 0.02$). The second order statistic $|G_{3\times3}|$ may provide a sensitive measure of ADC heterogeneity for ROI representing 9.4 × 9.4 × 30 mm or 2.6 cm^3 of lung tissue.

emphysema; chronic obstructive pulmonary disease; thoracic imaging; noble gas lung imaging

HYPERPOLARIZED ^{3}He magnetic resonance imaging (MRI) has emerged as a noninvasive imaging method for the evaluation of the regional distribution of anatomical and functional pulmonary changes associated with chronic obstructive pulmonary disease (COPD; Refs. 3, 11, 13, 20, 29). In particular, the measurement of the ^{3}He apparent diffusion coefficient (ADC; Ref. 29) has been exploited to probe the lung microstructure in patients with COPD (3, 11, 19, 20, 29) and in ex vivo explanted lungs (25, 27). Increases in ^{3}He ADC are consistent with expected increases in acinar size due to destruction of alveoli accompanying emphysema (19–21) and have been shown to correlate with histological measurements of disease (25, 27) and with age (7). The heterogeneity in values of ADC across the lung, measured using the ADC standard deviation (SD), has also been shown to be increased in subjects with COPD (14, 20), suggesting that there is a greater diversity of acinar and alveolar size in subjects with COPD compared with healthy volunteers. It is well established that in emphysema tissue heterogeneities exist (2, 9, 18) and several in vitro studies (4, 17, 24, 30) have shown that changes in tissue structure and composition are altered in emphysema and that these result in changes in tissue mechanics. In vivo, emphysematous changes also result in considerable radiological heterogeneity measurable using X-ray computed tomography (CT; Ref. 18). For example, areas of low attenuation in X-ray CT images of emphysematous patients (2) are believed to correspond to a distribution of regional disease.

One of the drawbacks of using the hyperpolarized whole lung mean ^{3}He ADC and ADC SD as a measure of lung tissue differences and heterogeneity is the resultant loss of regional information. With respect to the changes in ADC measures across the lung, postural ADC gradients have been reported (8, 23), and we (6) have also previously observed that regional ADC measures were dependent on disease status and location in the anterior-posterior as well as superior-inferior direction in subjects with stage III COPD (1) and healthy volunteers. Because in this region of interest (ROI) study we observed that both anatomical location and disease status provided significant and important contributions to regional ADC, we endeavored to develop a more sensitive, regional, second order statistic of ADC. For example, as shown in the schematic in Figure 1, for the ROI shown in *A* and *B*, the calculated ADC SD would be the same, but differences related to location can be readily appreciated and measured using a second order statistic. Accordingly, we postulated that a second order statistic of ADC gradients measured within the smallest ROI possible might provide an image-based and regional method of differentiating between healthy subjects and those with moderate and more severe disease. Moreover, the development of a method that could map ADC gradients across the lung might provide a visual tool to help identify both the magnitude and direction of such gradients, while preserving the regional context of the information, which is one of the major advantages of in vivo imaging.

Therefore, the purpose of this study was to develop and implement a method of mapping the changes in ADC (or ADC gradients) in the lung in healthy volunteers and subjects with COPD using a second order statistic and to show such gradients averaged in the slice plane in each and every nine-voxel ROI ($|G_{3\times3}|$; 9.4 × 9.4 × 30 mm tissue) across the lung. We present the first qualitative examples of such ADC gradient

Address for reprint requests and other correspondence: G. Parraga, Imaging Research Laboratories, Robarts Research Institute, 100 Perth Drive PO Box 5015, London Canada N6A 5K8 (e-mail: gep@imaging.robarts.ca).

The costs of publication of this article were defrayed in part by the payment of page charges. The article must therefore be hereby marked "*advertisement*" in accordance with 18 U.S.C. Section 1734 solely to indicate this fact.

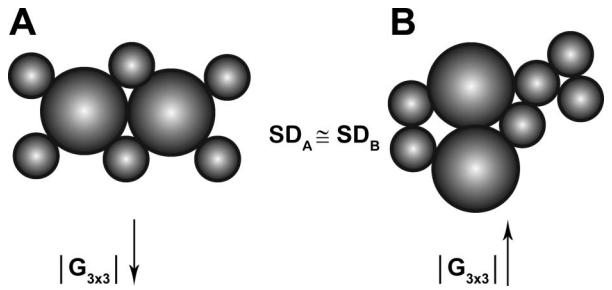

Fig. 1. Schematic tissue heterogeneity measurement. Two different regions of interest are shown in schematic *A* and *B* to show how the same apparent diffusion coefficients (ADC) SD provides different second order statistic or three-by-three voxel matrix ($|G_{3\times3}|$).

vector maps in a representative healthy subject and representative subjects with global initiative for chronic obstructive lung disease (GOLD) stage II (or moderate; Ref. 1) and stage III (or severe) COPD (1). In addition, a quantitative analysis of $|G_{3\times3}|$ for the center coronal slice is provided for 8 healthy volunteers and 16 subjects with COPD.

METHODS

Research subjects. Subjects were enrolled in this study based on their age and GOLD criteria (1) classification after providing written informed consent to the study protocol approved by the University of Western Ontario Standing Board of Human Research Ethics and Health Canada, as described previously (6, 16). COPD subjects required a disease diagnosis of at least 1 yr, having had a smoking history of at least 10 pack-years and fewer than 3 exacerbations within the last 12 mo. Healthy subjects were included if they had no history of chronic respiratory disease, less than one pack-year smoking history, forced expiratory volume in 1 s (FEV_1) >80% predicted, FEV_1 divided by the forced vital capacity (FVC) or FEV_1/FVC >70%, and no current diagnosis or history of cardiovascular disease. Throughout the duration of the study, COPD subjects were to be withdrawn from the study if they experienced a COPD exacerbation. COPD subjects were categorized according to the GOLD criteria (1), based on postbronchodilator FEV_1 as moderate or stage II (FEV_1 >50% and <80% predicted) and severe or stage III (FEV_1 >30% and <50% predicted).

Study assessments. After subjects provided written, informed consent, they were screened for MRI and coil compatibility and underwent a physical exam, plethysmography, and spirometry. Spirometry and plethysmography were performed in the morning after patients delayed inhaled bronchodilators and corticosteroids for ~12 h. Briefly, spirometry was performed pre- and postbronchodilator using an ndd EasyOne spirometer (ndd Medizintchnik AG, Zurich, CH) reporting FEV_1 (absolute and percent predicted) and FVC. Whole body plethysmography (SensorMedics VIASYS Healthcare, Yorba Linda, CA) was also performed at the pulmonary function laboratory at University Hospital (London Health Sciences Centre, London, Canada) for the measurement of total lung capacity, residual volume, and functional residual capacity.

MRI. MRI was performed on a whole body 3.0 Tesla Excite 12.0 MRS system [General Electric Health Care (GEHC), Durham, NC] with broadband imaging capability as described previously (6, 16). All helium imaging used a whole body gradient set with maximum gradient amplitude of 1.94 G/cm and a single channel, elliptical transmit/receive chest coil (RAPID Biomedical GmbH, Wuerzburg, Germany). The basis frequency of the coil was 97.3 MHz, and the excitation power was 3.2 kW using an AMT 3T90 RF power amplifier (GEHC). ^{3}He multislice images were obtained in the coronal plane using a fast gradient-recalled echo method with centric k-space sampling. Two interleaved images [echo time (TE) = 3.7 ms, relaxation time (TR) = 7.6 ms, 128 × 128, 7 slices, 30-mm thick, field of view (FOV) = 40 × 40 cm] without and with additional diffusion sensitization (gradient = 1.94 G/cm, rise and fall time = 0.5 ms, duration = 0.46 ms, b value = 1.6 s/cm^2) were acquired for each slice. All scanning was completed within ~10 min of subjects first lying in the scanner. Hyperpolarized ^{3}He gas was provided by a turn-key, spin-exchange optical pumping system (HeliSpin, GEHC) as described previously (6, 16). Briefly, in a typical study this system provided 30% polarization in 12 h. Doses (5 ml/kg) were delivered in 1-liter plastic bags (Tedlar, Jensen Inert Products, Coral Springs, FL) diluted with ultrahigh purity, medical-grade nitrogen (Spectra Gases, Alpha, NJ) so that the total volume of gas inhaled for each subject was 1 liter. Polarization of the diluted dose was quantified by a polarimetry station (GEHC). ^{3}He MR scans were acquired during an inhalation breathhold after inspiration from a tidal volume of the 1-liter volume of ^{3}He mixed with N_2 (5 ml/kg dose).

Image analysis. ^{3}He MRI images were analyzed by a single observer and ADC was calculated on a pixel-by-pixel basis with a b value of 1.6 s/cm^2, as described previously (6, 16). To summarize briefly, all image slices were previously analyzed for ADC (6), but for this investigation, only the center coronal slice for each individual subject was assessed, where the center slice image was chosen based on the location of the carina. After the trachea and major airways were segmented and removed, the mean ADC and SD of ADC for the entire slice were calculated. The diffusion-weighted images were analyzed by a single trained observer in an image visualization environment (digital copy) with room-lighting levels equivalently established for all image analysis sessions. Mean ADC and ADC maps were processed using an in-house software programmed in the IDL Virtual Machine platform (Research Systems, Denver, CO) as described previously (6, 16).

ADC gradients. A schematic of the methodology developed to calculate ADC gradient vectors is provided in Fig. 2. To summarize, the vector gradient (local rate of change in ADC value) as shown in an ADC map (Fig. 2*A*) was quantified in a three-by-three voxel-by-voxel ROI (Fig. 2*B*) and displayed using ADC vector gradient maps (Fig. 2*C*). Thus differences in ADC within an ROI were calculated and expressed as both magnitude and direction of ADC gradient. Accordingly, in the ADC gradient vector map shown in Fig. 2, vectors in voxel locations represent both the magnitude and direction of local ADC gradients for that ROI. A representative calculation is shown in Fig. 2, where $a_{i,j}$ is the ADC value at location *i,j* in the image.

The vector gradient in ADC values at *i,j* is given by:

$$\bar{G}_{i,j} = Gx_{i,j}\hat{x} + Gy_{i,j}\hat{y} \quad (1)$$

where *x* and *y* are unit vectors and $Gx_{i,j}$ and $Gy_{i,j}$ are the average *x* and *y* direction vector components given by:

$$Gx_{i,j} = \frac{1}{6\Delta}[a_{i+1,j+1} + a_{i+1,j} + a_{i+1,j-1} - a_{i-1,j+1} - a_{i-1,j} - a_{i-1,j-1}] \quad (2)$$

and

$$Gy_{i,j} = \frac{1}{6\Delta}[a_{i+1,j+1} + a_{i,j+1} + a_{i-1,j+1} - a_{i+1,j-1} - a_{i,j-1} - a_{i-1,j-1}] \quad (3)$$

where the pixel size is Δ = 3 mm in both *x* and *y* directions.

The gradient magnitudes and directions are given by:

$$|G_{i,j}| = \sqrt{|Gx_{i,j}|^2 + |Gy_{i,j}|^2} \quad (4)$$

and

$$\theta = \arctan\frac{Gy}{Gx} \quad (5)$$

A representative "quiver plot" (Matlab 6.5, The Mathworks, Natick, MA) of ADC vector gradient is shown in Fig. 2*C*.

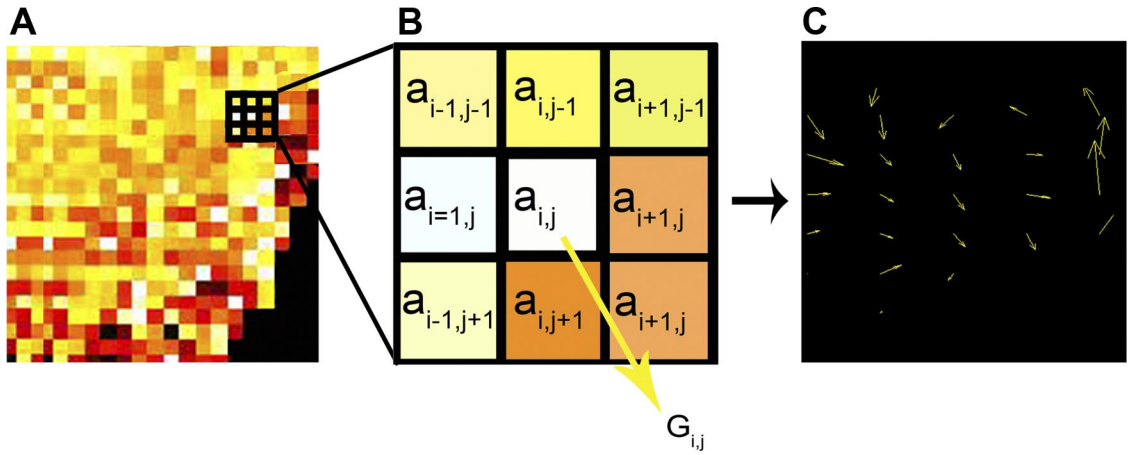

Fig. 2. Schematic of ^{3}He ADC gradient vector methodology. *A*: ADC map and region of interest from which ADC gradient vectors were calculated. *B*: representative region of interest three-by-three voxel matrix from ADC map with resultant calculated vector, $G_{i,j}$, which summarizes magnitude and direction of ADC gradient. *C*: resulting ADC vector map corresponding to ADC map in *A*.

All coronal slices were acquired with 30-mm thickness, and, therefore, the ADC value in the z direction was accordingly an average over this 30-mm thick slice. Before the ADC map was evaluated for the generation of vectors, image noise was filtered (out of the Bo image) by applying a hanning filter to the k-space data thereby applying a noise threshold to the resulting image. The hanning filter is a narrow band filter that helped suppress noise and enhanced signal in k-space and did not effect the ADC calculation. After the image noise filter was applied and an ADC map was created, an ADC map filter was used to create the vector maps. This filter worked by refusing to calculate an ADC gradient for any three-by-three voxel ROI where at least one voxel value was <0.05 cm^2/s. The value of 0.05 cm^2/s was empirically set as a threshold for edge voxels (such as those on the edge of an unventilated portion of an image), because this value was two SDs below the mean ADC of healthy subjects. Therefore, edge voxels were defined as those voxels with a neighboring voxel value <0.05 cm^2/s and were not included in the analysis.

Statistical analysis. Mean $|G_{i,j}|$ values for three-by-three voxel matrices ($|G_{3\times3}|$) were calculated using Matlab 6.5 (Mathworks, Natick, MA). All statistical analyses were performed using the SPSS 15.0 statistical package (LEAD Technologies, Chicago, IL). Statistical comparisons of mean ADC, SD of ADC, and $|G_{3\times3}|$ were conducted using the one-way ANOVA, and multiple comparisons between subject subgroups were performed using the Fisher's least significant difference test. Levene's test was used to ensure equality of variance between groups. In all statistical analyses, results were considered significant when the probability of making a Type I error was $<5\%$ ($P < 0.05$).

RESULTS

Research subjects. Demographic characteristics for all 24 subjects enrolled and evaluated in this study (15 male) are provided in Table 1 with very similar mean ages and age ranges for each subgroup. No subjects were withdrawn from the study due to COPD exacerbations. As the COPD subjects and healthy volunteers were enrolled based upon FEV_1 and FEV_1/FVC according to GOLD criteria (1), the mean values for FEV_1 and FEV_1/FVC for each subject subgroup reflect the GOLD criteria categorization. In addition to the expected and significantly decreased FEV_1 and FEV_1/FVC for the COPD subgroups compared with the healthy volunteers ($P < 0.01$), the baseline functional residual capacity was significantly increased for both COPD subject groups ($P < 0.01$) and the total lung capacity was also significantly increased for the stage III COPD subgroup only ($P < 0.001$), both findings consistent with lung hyperinflation. Baseline residual volume was also significantly increased for the stage III COPD subgroup ($P < 0.001$), which is consistent with gas trapping.

ADC and ADC gradients. Figure 3 shows ^{3}He MR images (Fig. 3*A*), corresponding ^{3}He ADC maps (Fig. 3*B*) and corresponding ADC histograms (Fig. 3*C*) for three representative study subjects including a healthy elderly subject (shown in Fig. 3, *A–C*, *i*), a subject with stage II COPD (shown in Fig. 3, *A–C*, *ii*), and a subject with stage III COPD (shown in Fig. 3, *A–C*, *iii*).

Figure 4*A* shows the results of the calculation of ADC gradients across each and every contiguous three-by-three or nine-voxel matrix (9.4 × 9.4 × 30 mm) as a ^{3}He MRI ADC gradient vector map for the same representative subjects shown in Fig. 3. The magnitude and direction of the ADC gradients are displayed as yellow vectors that show regional differences

Table 1. *Subject demographics*

	Healthy Volunteers (n = 8)	Stage II (Moderate) COPD (n = 9)	Stage III (Severe) COPD (n = 7)	All Subjects (n = 24)
Age, yr (±SD)	67 (6)	68 (5)	66 (8)	67 (7)
Male sex	5	4	6	15
FEV_1, % (±SD)*	106 (19)	63 (8)	42 (7)	73 (35)
IC, % (±SD)*	111 (160)	99 (18)	78 (17)	96 (22)
FRC, % (±SD)*	95 (14)	116 (14)	152 (37)	120 (32)
RV, % (±SD)*	97 (10)	142 (20)	188 (55)	145 (48)
TLC, % (±SD)*	104 (19)	108 (9)	115 (23)	109 (15)

COPD, chronic obstructive pulmonary disease; FEV_1, forced expiratory volume in 1 s; IC, inspiratory capacity; FRC, functional residual capacity; RV, residual volume; TLC, total lung capacity. *Predicted.

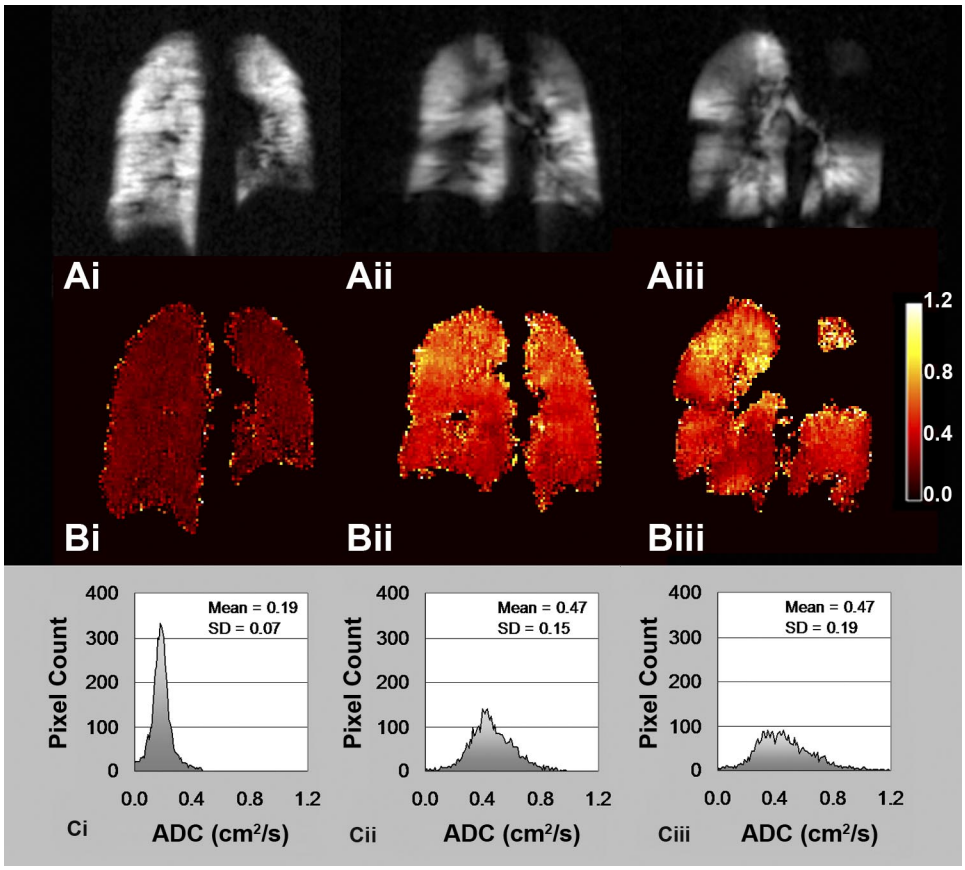

Fig. 3. ^{3}He MRI center coronal slice ADC analysis. *A*: ^{3}He MR images of a healthy volunteer (*i*), a subject with stage II (moderate) chronic obstructive pulmonary disease (COPD; *ii*), and a subject with stage III (severe) COPD (*iii*). *B*: ^{3}He ADC maps of a healthy volunteer (*i*), a subject with stage II (moderate) COPD (*ii*), and subject with stage III (severe) COPD (*iii*). *C*: ^{3}He ADC histograms of a healthy volunteer (*i*), a subject with stage II (moderate) COPD (*ii*), and a subject with stage III (severe) COPD (*iii*).

in local ADC gradients across the center coronal slice. In Fig. 4*B*, a histogram analysis of $|G_{3\times3}|$ values shown in the map in Fig. 4*A* is provided and these show the mean $|G_{3\times3}|$ and $|G_{3\times3}|$ SD for each of the representative subjects.

Table 2 provides a summary of the results for all subjects by subgroup for mean ADC, ADC SD, and mean $|G_{3\times3}|$, $|G_{5\times5}|$, and $|G_{7\times7}|$. The difference in mean ADC was significantly different between the subgroup of healthy volunteers and subjects with

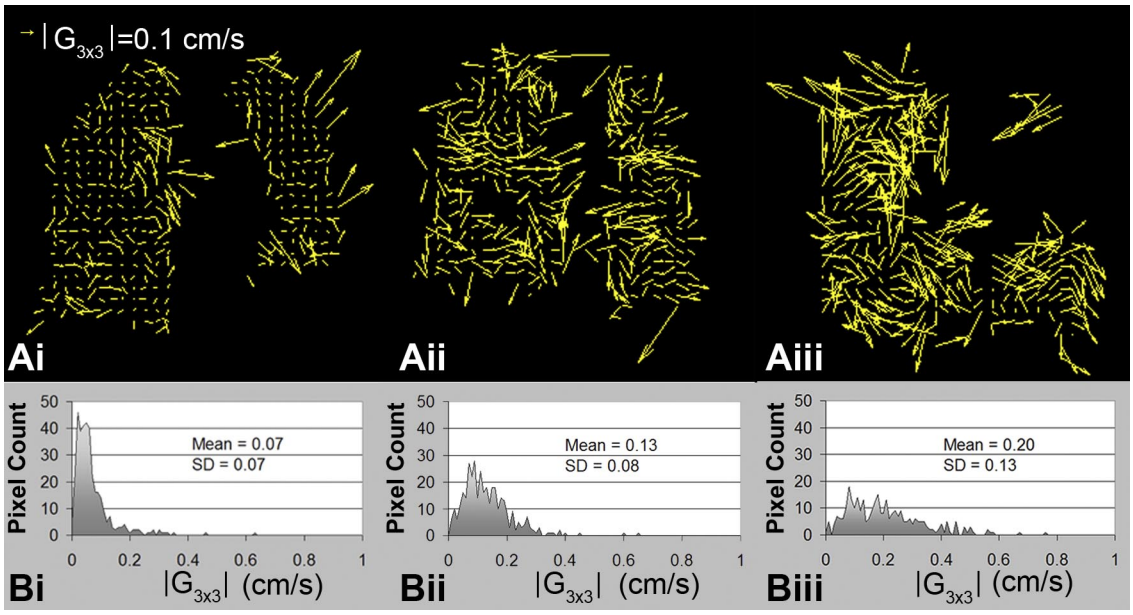

Fig. 4. ^{3}He MRI ADC gradient vector maps. *A*: ADC $|G_{3\times3}|$ gradient vector map for a representative healthy volunteer (*i*), a subject with stage II (moderate) COPD (*ii*), and a subject with stage III (severe) COPD (*iii*). *B*: ADC $|G_{3\times3}|$ gradient vector histograms for a representative healthy volunteer (*i*), a subject with stage II (moderate) COPD (*ii*), and a subject with stage III (severe) COPD (*iii*).

stage II COPD ($P < 0.05$) and stage III COPD ($P < 0.01$) but not between the subgroup with stage II and subgroup with stage III COPD. The ADC SD was also not significantly different between subject subgroups with stage II and stage III COPD or between healthy volunteers and subjects with stage II COPD. However, for mean $|G_{3\times3}|$, there was a statistically significant difference between subjects with stage II (0.14 ± 0.03 cm/s) and stage III COPD (0.19 ± 0.03 cm/s, $P < 0.005$) and between healthy volunteers (0.12 ± 0.03 cm/s) and subjects with stage II ($P < 0.02$) and stage III COPD ($P < 0.0001$). The results (Table 2) for $|G_{5\times5}|$ and $|G_{7\times7}|$ are also similar to those observed for $|G_{3\times3}|$. Figure 5 provides a direct comparison of mean ADC and mean $|G_{3\times3}|$ for each of the subgroups by subject.

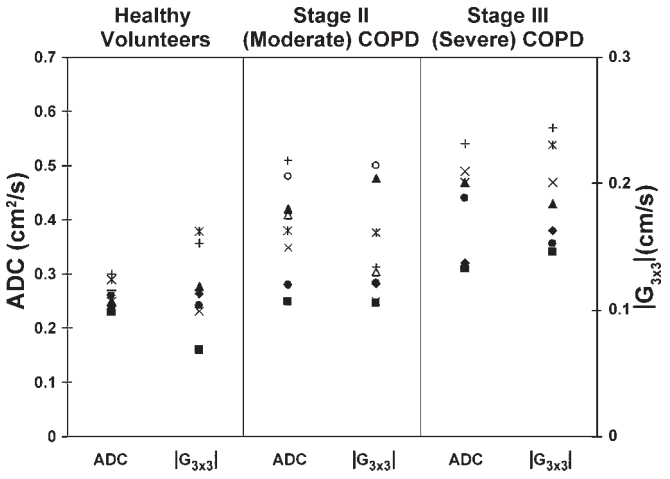

Fig. 5. Mean ^{3}He ADC and mean $|G_{3\times3}|$ for all subjects by subgroup. Mean ADC and $|G_{3\times3}|$ by subject subgroup. Subjects with stage III (severe) COPD statistically significantly different than subjects with stage II (moderate) COPD ($P < 0.005$) and healthy volunteers ($P < 0.0001$).

DISCUSSION

A central challenge in our understanding of COPD progression is an in vivo description of how and where specific changes in airways and air spaces are occurring over time. While COPD is recognized as a heterogeneous lung disease (18), it is typically diagnosed on the basis of global lung function, such as spirometry and diffusing capacity for carbon monoxide, and, less routinely, lung tissue destruction is measured as low attenuation areas using X-ray CT (2, 12, 22, 26). The hyperpolarized ^{3}He MRI ADC has been shown to correlate with histological measurements of emphysematous disease (25, 28) ex vivo. As the ^{3}He ADC provides an average value for the subvoxel contributions of both airways and air spaces to ^{3}He diffusion, we hypothesized that a regional second order statistic of ADC could be developed to provide an in vivo measurement of regional heterogeneity of disease. In addition, we postulated that such ^{3}He ADC gradients could provide a novel in vivo filter capable of discriminating between COPD subgroups with different disease severities. Accordingly, our goal was to develop an in vivo measure of regional lung disease heterogeneity in COPD patients, based on the measurement of the ^{3}He ADC using hyperpolarized ^{3}He MRI. Toward achieving this goal, we present *1*) the development of an ADC gradient vector mapping method based on a nine-voxel average ($9.4 \times 9.4 \times 30$ mm), *2*) the application of this mapping method to qualitatively display regional ADC heterogeneity in elderly healthy volunteers and subjects with COPD, and *3*) calculation of a quantitative second order statistic, ($|G_{3\times3}|$), that provides the mean of such gradients averaged over each and every nine-voxel ROI across the lung.

The ADC gradient maps depicting vector gradients for nine-voxel ROI provide a qualitative determination of airway and air space heterogeneity in small ROI that correspond to 2.6 cm^3 of lung tissue. A design-based stereological approach (15) recently estimated the mean size of a single normal alveolus to be 4.2×10^{-6} cm^3 irrespective of lung size. According to these calculations, the ADC gradients calculated here correspond to the contributions of ~500,000–600,000 alveoli within the 2.6-cm^3 voxel matrix. The gradient maps provide a visual snapshot of the heterogeneity of the contributing alveoli and airways to the calculated ADC using the $|G_{3\times3}|$ filter. These maps also provide the ability to determine qualitative differences between subjects and within the lung of individual subjects. The ADC $|G_{3\times3}|$ shown in Fig. 4 and summarized in Table 2 also provides a new second order statistic that describes the mean magnitude of the ADC gradients within the 2.6-cm^3 voxel, which like the ADC SD, provides a measure of ADC heterogeneity. However, as shown in Table 2, $|G_{3\times3}|$ is significantly different between stage II COPD and stage III COPD ($P < 0.005$), unlike SD of ADC, which is not significantly different between COPD subgroups. The preservation of regional context in $|G_{3\times3}|$ may have resulted in this difference in sensitivity between ADC SD and ADC $|G_{3\times3}|$ observed.

Previous to this work, the age dependence (7) and anatomical dependence (6, 8, 23) of the ^{3}He ADC has been shown. The finding here of significantly different ADC gradients in 2.6 cm^3 voxels in stage II and stage III COPD subjects suggests that aggressive destruction of parenchyma is regionally more heterogeneous as disease severity (measured using spirometry) increases.

Table 2. *^{3}He ADC gradients*

	Healthy Volunteers (n = 8)	Stage II (Moderate) COPD (n =9)	Stage III (Severe) COPD (n = 7)	Significance of Difference (P Value)		
				HV-M	HV-S	M-S
Mean ADC, cm^2/s (±SD)*	0.25 (0.02)	0.37 (0.1)	0.42 (0.1)	$P < 0.05$	$P < 0.01$	$P > 0.2$
SD ADC, cm^2/s (±SD)*	0.18 (0.02)	0.22 (0.08)	0.26 (0.09)	$P > 0.1$	$P < 0.01$	$P > 0.1$
$\|G_{3\times3}\|$, cm/s (±SD)*	0.12 (0.03)	0.14 (0.03)	0.19 (0.03)	$P < 0.02$	$P < 0.0001$	$P < 0.005$
$\|G_{5\times5}\|$, cm/s (±SD)*	0.12 (0.03)	0.15 (0.06)	0.18 (0.03)	$P < 0.003$	$P < 0.0001$	$P = 0.05$
$\|G_{7\times7}\|$, cm/s (±SD)*	0.12 (0.03)	0.16 (0.06)	0.20 (0.06)	$P < 0.02$	$P < 0.0001$	$P < 0.005$

*Bracketed values are SD of the mean for the subgroup. HV, healthy volunteers; M, subjects with stage II (moderate) COPD; S, subjects with Stage III (severe) COPD.

One of the limitations of this study includes the small group of subjects in which we piloted this approach. The large-scale application of this method to a larger group of healthy volunteers of various ages and those with stage I COPD will be required to assess $|G_{3\times3}|$ differences within subjects with less severe and no apparent disease and to visualize and quantify gradients over time as disease progresses. An important consideration to note is that the method of deriving ADC $|G_{3\times3}|$ developed in this study uses rather thick slices generated by diffusion-weighted imaging (30 mm), which results in $|G_{3\times3}|$ reflecting a rather large (9.1 $\times$ 9.1 $\times$ 30 mm) anisotropic voxel. The filter provided by $|G_{3\times3}|$ enables a measurement of heterogeneity within the voxel measured and across the lung slice; however, three-dimensional imaging approaches with thinner slices would allow for the determination of heterogeneity in smaller and less anisotropic voxels, perhaps yielding even more information and with greater sensitivity. In other words, thinner slices would allow for the derivation of smaller filters to discern potential heterogeneity differences within smaller ROI. We note that we also determined ADC $|G_{5\times5}|$, $|G_{7\times7}|$, and $|G_{9\times9}|$ and observed the same mean values for the subgroups as were determined for $|G_{3\times3}|$. This result suggests that smaller filter sizes may provide greater sensitivity to differences in these subgroups.

One of the original rationales for deriving $|G_{3\times3}|$ was to assess ADC gradients around the perimeter of ventilation defects as a way to measure lung structural heterogeneity near areas of the lung that are unable participate in ventilation within the timeframe of MR image acquisition (14–16 s). The derivation of $|G_{3\times3}|$ from images acquired with thinner slices and smaller voxels may help in this regard. The issue of unventilated or less ventilated lungs within the timeframe of MR image acquisition leads to the description of a major fundamental limitation of the approach developed here, which relates to the fact that the measurement of ADC and ADC gradients is dependent on the ADC signal from a well-ventilated lung. Hence, ADC $|G_{3\times3}|$ ignores the contributions of those areas of the lung that are unable to participate in ventilation due to bullous disease, mucous plugs, or airway narrowing or collapse. Thus this approach can only reflect heterogeneity in areas of the lung that still participate in ventilation which provides a distinct bias to the results. In this regard, an important next step will be to assess correlations between $|G_{3\times3}|$ from MRI and quantitative CT as well as histological sections.

There is evidence from animal models (10) and from patient studies (5) suggesting that emphysematous destruction results in increased SD and coefficients of variation of alveolar diameters and area over time: both suggestive of increased heterogeneity of alveolar size as the disease progresses. The ability, provided by hyperpolarized ^{3}He MRI, to quantitatively and noninvasively measure the extent, location, and localized gradients in emphysema has the potential to provide important physiological information in individual COPD subjects and subgroups for *1*) earlier detection of disease changes and mapping of changes that accompany disease progression, *2*) identification of regional changes after pharmaceutical intervention, and *3*) identification of localized disease extent and severity before and as a way to plan for radiation, pharmaceutical, surgical, and bronchoscopic interventions. In this regard, the second order statistic we describe here provides a way to sensitively and quantitatively measure localized ADC gradients, while preserving the regional information provided by imaging. We are currently evaluating the use of this measurement in the longitudinal assessment of COPD subjects, which will provide critical information regarding potential changes in such gradients in individual subjects and subject subgroups over time. Our working hypothesis based on the current results is that subjects with stage II and stage III COPD (who have stopped smoking) will show increased $|G_{3\times3}|$ over relatively short periods of time (1–2 yr) without changes in spirometric measurements of disease. We are also directly applying this method to data sets acquired with thin slices to assess regional heterogeneity around large ventilation defects with comparison to CT.

In summary, the ADC gradient maps provide a way to qualitatively visualize ADC heterogeneity, providing a new way to evaluate the temporal and spatial dynamics of emphysema within the lung using ^{3}He MRI. Visualization of the quantitative vectors helps identify both the magnitude and direction of such gradients, while preserving regional context. As a first step in the development and application of this method, qualitative representative examples of such ADC gradient vector maps in a healthy subject and subjects with stage II and stage III COPD are provided. In addition, a quantitative analysis of the mean magnitude of $|G_{3\times3}|$ is provided for 8 healthy volunteers and 16 subjects with COPD, which provided a means of differentiating subjects with stage III and stage II COPD. The method evaluated in this study may provide a means of tracking changes in emphysema over time in vivo, which can complement (and are certainly more practicable in patients than) histological studies.

ACKNOWLEDGMENTS

We thank S. Halko, S. McKay, and C. Piechowicz for clinical coordination and clinical database management; W. Lam and A. Wheatley for production and dispensing of ^{3}He gas; and E. Lorusso and C. Harper-Little for MR scanning of research volunteers. We also acknowledge assistance from A. Wheatley with programming. Helpful discussions with Dr. I. A. Cunningham and A. Fenster also contributed significantly to the manuscript.

GRANTS

A. Evans was provided with salary funding support from the Western Graduate Research Fund provided by the University of Western Ontario (London Canada), a Fellowship from the Canadian Institutes of Health Research Vascular Research Training Program (London, Canada), and a research bursary from McGill University (Dr. McLeod Memorial Scholarship, McGill University, Montreal Canada). The study was also supported by funding from the Ontario Research and Development Challenge Fund and the Canadian Institutes of Health Research.

DISCLOSURES

We acknowledge the use of two onsite hyperpolarized ^{3}He gas polarizer systems (HeliSpin, GEHC), which were provided to Robarts Research Institute by Merck through an agreement between GEHC and Merck, as well as funding from Merck Frosst Canada Limited and the Imaging Department at Merck Research Laboratories.

REFERENCES

1. **Anonymous.** *Global Strategy For The Diagnosis, Management, And Prevention Of Chronic Obstructive Pulmonary Disease. Global Initiative For Chronic Obstructive Lung Disease* (Report update for 2007).
2. **Baldi S, Miniati M, Bellina CR, Battolla L, Catapano G, Begliomini E, Giustini D, Giuntini C.** Relationship between extent of pulmonary emphysema by high-resolution computed tomography and lung elastic

recoil in patients with chronic obstructive pulmonary disease. *Am J Respir Crit Care Med* 164: 585–589, 2001.

3. **de Lange EE, Mugler JP, III, Brookeman JR, Knight-Scott J, Truwit JD, Teates CD, Daniel TM, Bogorad PL, Cates GD.** Lung air spaces: MR imaging evaluation with hyperpolarized ^{3}He gas. *Radiology* 210: 851–857, 1999.
4. **Dolhnikoff M, Mauad T, Ludwig MS.** Extracellular matrix and oscillatory mechanics of rat lung parenchyma in bleomycin-induced fibrosis. *Am J Respir Crit Care Med* 160: 1750–1757, 1999.
5. **Dunnill MS.** Quantitative methods in the study of pulmonary pathology. *Thorax* 17: 320–328, 1962.
6. **Evans A, McCormack D, Ouriadov A, Etemad-Rezai R, Santyr G, Parraga G.** Anatomical distribution of (3)He apparent diffusion coefficients in severe chronic obstructive pulmonary disease. *J Magn Reson Imaging* 26: 1537–1547, 2007.
7. **Fain SB, Altes TA, Panth SR, Evans MD, Waters B, Mugler JP, III, Korosec FR, Grist TM, Silverman M, Salerno M, Owers-Bradley J.** Detection of age-dependent changes in healthy adult lungs with diffusion-weighted ^{3}He MRI. *Acad Radiol* 12: 1385–1393, 2005.
8. **Fichele S, Woodhouse N, Swift AJ, Said Z, Paley MN, Kasuboski L, Mills GH, Van Beek EJ, Wild JM.** MRI of helium-3 gas in healthy lungs: posture related variations of alveolar size. *J Magn Reson Imaging* 20: 331–335, 2004.
9. **Hubmayr RD.** Perspective on lung injury and recruitment: a skeptical look at the opening and collapse story. *Am J Respir Crit Care Med* 165: 1647–1653, 2002.
10. **Ito S, Ingenito EP, Arold SP, Parameswaran H, Tgavalekos NT, Lutchen KR, Suki B.** Tissue heterogeneity in the mouse lung: effects of elastase treatment. *J Appl Physiol* 97: 204–212, 2004.
11. **Kauczor HU, Ebert M, Kreitner KF, Nilgens H, Surkau R, Heil W, Hofmann D, Otten EW, Thelen M.** Imaging of the lungs using ^{3}He MRI: preliminary clinical experience in 18 patients with and without lung disease. *J Magn Reson Imaging* 7: 538–543, 1997.
12. **Lucey EC, Keane J, Kuang PP, Snider GL, Goldstein RH.** Severity of elastase-induced emphysema is decreased in tumor necrosis factor-alpha and interleukin-1beta receptor-deficient mice. *Lab Invest* 82: 79–85, 2002.
13. **Moller HE, Chen XJ, Saam B, Hagspiel KD, Johnson GA, Altes TA, de Lange EE, Kauczor HU.** MRI of the lungs using hyperpolarized noble gases. *Magn Reson Med* 47: 1029–1051, 2002.
14. **Morbach AE, Gast KK, Schmiedeskamp J, Dahmen A, Herweling A, Heussel CP, Kauczor HU, Schreiber WG.** Diffusion-weighted MRI of the lung with hyperpolarized helium-3: a study of reproducibility. *J Magn Reson Imaging* 21: 765–774, 2005.
15. **Ochs M, Nyengaard JR, Jung A, Knudsen L, Voigt M, Wahlers T, Richter J, Gundersen HJ.** The number of alveoli in the human lung. *Am J Respir Crit Care Med* 169: 120–124, 2004.
16. **Parraga G, Ouriadov A, Evans A, McKay S, Lam WW, Fenster A, Etemad-Rezai R, McCormack D, Santyr G.** Hyperpolarized ^{3}He ventilation defects and apparent diffusion coefficients in chronic obstructive pulmonary disease: preliminary results at 3.0 Tesla. *Invest Radiol* 42: 384–391, 2007.
17. **Rocco PR, Negri EM, Kurtz PM, Vasconcellos FP, Silva GH, Capelozzi VL, Romero PV, Zin WA.** Lung tissue mechanics and extracellular matrix remodeling in acute lung injury. *Am J Respir Crit Care Med* 164: 1067–1071, 2001.
18. **Russi EW, Bloch KE, Weder W.** Functional and morphological heterogeneity of emphysema and its implication for selection of patients for lung volume reduction surgery. *Eur Respir J* 14: 230–236, 1999.
19. **Saam BT, Yablonskiy DA, Kodibagkar VD, Leawoods JC, Gierada DS, Cooper JD, Lefrak SS, Conradi MS.** MR imaging of diffusion of (3)He gas in healthy and diseased lungs. *Magn Reson Med* 44: 174–179, 2000.
20. **Salerno M, Altes TA, Brookeman JR, de Lange EE, Mugler JP III.** Dynamic spiral MRI of pulmonary gas flow using hyperpolarized (3)He: preliminary studies in healthy and diseased lungs. *Magn Reson Med* 46: 667–677, 2001.
21. **Salerno M, de Lange EE, Altes TA, Truwit JD, Brookeman JR, Mugler JP III.** Emphysema: hyperpolarized helium 3 diffusion MR imaging of the lungs compared with spirometric indexes–initial experience. *Radiology* 222: 252–260, 2002.
22. **Snider GL, Lucey EC, Stone PJ.** Animal models of emphysema. *Am Rev Respir Dis* 133: 149–169, 1986.
23. **Swift AJ, Wild JM, Fichele S, Woodhouse N, Fleming S, Waterhouse J, Lawson RA, Paley MN, Van Beek EJ.** Emphysematous changes and normal variation in smokers and COPD patients using diffusion ^{3}He MRI. *Eur J Radiol* 54: 352–358, 2005.
24. **Tanaka R, Al Jamal R, Ludwig MS.** Maturational changes in extracellular matrix and lung tissue mechanics. *J Appl Physiol* 91: 2314–2321, 2001.
25. **Tanoli TS, Woods JC, Conradi MS, Bae KT, Gierada DS, Hogg JC, Cooper JD, Yablonskiy DA.** In vivo lung morphometry with hyperpolarized ^{3}He diffusion MRI in canines with induced emphysema: disease progression and comparison with computed tomography. *J Appl Physiol* 102: 477–484, 2007.
26. **Vlahovic G, Russell ML, Mercer RR, Crapo JD.** Cellular and connective tissue changes in alveolar septal walls in emphysema. *Am J Respir Crit Care Med* 160: 2086–2092, 1999.
27. **Woods JC, Choong CK, Yablonskiy DA, Bentley J, Wong J, Pierce JA, Cooper JD, Macklem PT, Conradi MS, Hogg JC.** Hyperpolarized ^{3}He diffusion MRI and histology in pulmonary emphysema. *Magn Reson Med* 56: 1293–1300, 2006.
28. **Woods JC, Yablonskiy DA, Choong CK, Chino K, Pierce JA, Hogg JC, Bentley J, Cooper JD, Conradi MS, Macklem PT.** Long-range diffusion of hyperpolarized ^{3}He in explanted normal and emphysematous human lungs via magnetization tagging. *J Appl Physiol* 99: 1992–1997, 2005.
29. **Yablonskiy DA, Sukstanskii AL, Leawoods JC, Gierada DS, Bretthorst GL, Lefrak SS, Cooper JD, Conradi MS.** Quantitative in vivo assessment of lung microstructure at the alveolar level with hyperpolarized ^{3}He diffusion MRI. *Proc Natl Acad Sci USA* 99: 3111–3116, 2002.
30. **Yuan H, Kononov S, Cavalcante FS, Lutchen KR, Ingenito EP, Suki B.** Effects of collagenase and elastase on the mechanical properties of lung tissue strips. *J Appl Physiol* 89: 3–14, 2000.